Radio Positioning and Tracking of High-Speed Devices in 5G NR Networks: System Concept and Performance

Jukka Talvitie*, Mike Koivisto*, Toni Levanen*, Tero Ihalainen†, Kari Pajukoski†, and Mikko Valkama*
* Department of Electrical Engineering, Tampere University, Finland
†Nokia Bell Labs, Finland
Email: jukka.talvitie@tuni.fi

***Abstract*—This paper addresses high-efficiency radio positioning and tracking of high-speed objects in emerging fifth generation (5G) new radio (NR) networks. Methods and system concept are described, building on network side reference signal measurements and data fusion and tracking. Also realistic performance results are provided and analyzed, in the context of mmWave NR deployment for high-speed trains at 30 GHz carrier frequency. It is shown that below 3 m positioning accuracy can be achieved with 95% availability, which fits in the positioning performance requirements for traffic monitoring and control, as specified by the 3rd generation partnership project (3GPP). Moreover, the given positioning performance can be achieved without assuming clock synchronization between the baseband units (BBUs) at the network side. In fact, the proposed approach enables sub-nanosecond estimation accuracy of network clock offsets, which benefits various radio resource management (RRM) functionalities of the network for increased spectral efficiency.**

***Index Terms*—Positioning, Synchronization, Fifth generation mobile networks, 5G, New Radio, NR, High-speed trains, HST**

I. Introduction

The upcoming fifth generation (5G) new radio (NR) technologies introduce a vast set of new industry verticals, which have potential to revolutionize the ongoing digitalization for future society. With numerous new features and flexible radio interface parametrization, including adjustable subcarrier spacing, the performance of 5G NR networks can be optimized particularly for various use cases. Furthermore, positioning has been considered as one of the key features in the new 5G NR networks, which offers added value for many 5G verticals and facilitates specific mission-critical services, as well as allows location-aware communications and radio resource management (RRM) for improved spectral efficiency, as discussed in [1] and [2].

As presented in [3], transportation systems are considered as one of the new use cases enabled by the 5G technology, which is able to introduce various new features, such as high reliability and low-latency, for increased efficiency and safety. Such use cases include, for example, the high-speed train (HST) scenario and the highway scenario, presented in [4]. In these types of scenarios, it is typical that the network includes a distinct geometrical structure, where the network transceivers are aligned along the given vehicle paths. Consequently, this introduces specific radio wave propagation characteristics and a unique system geometry, which is especially crucial for radio-based positioning.

Positioning in 5G networks has been earlier studied, for example, in [5]–[9], in which the latter focuses on the HST scenario. In this paper, we introduce a novel 5G positioning approach for high-speed vehicles by utilizing time difference of arrival (TDoA) and angle-of-arrival (AoA) measurements in order to achieve high-performance positioning and tracking without demanding network synchronization. Moreover, as a by-product, the proposed approach produces clock-offset estimates for the network nodes, which can be utilized in various RRM related network functionalities for increased performance. In this paper, in order to illustrate the positioning and tracking performance, we focus on the HST scenario by considering a part of the Shanghai-Beijing high-speed railway. Based on the 5G NR signal structures and channel models, provided in [10] and [11], it is shown that the proposed approach, including asynchronous TDoA and AoA measurements together with extended Kalman filter (EKF) based vehicle tracking, is able to meet the positioning accuracy requirements for traffic monitoring and control, as specified by the 3rd generation partnership project (3GPP) in [3]. The considered approach assumes that the positioning is performed at the network side, which ensures that the most recent and low-latency position information is always available at the network side, as favored in several mission-critical use cases, such as autonomous trains.

The rest of the paper is organized as follows. Section II describes the considered system model with received signal structures. In Section III, the methods for obtaining the TDoA and AoA measurements are presented, whereas in Section IV, the considered EKF tracking algorithm is introduced. Finally, the performance of the proposed approach is evaluated in section V, and the conclusions are drawn in Section VI.

II. System Model

We consider a HST scenario based on the high-speed network deployment given in [4, Section 6.1.5]. The network consists of RRHs, which are located along the railway track at 580

This work was supported by the Doctoral Program of the President of Tampere University of Technology, and by the Finnish Funding Agency for Technology and Innovation (Business Finland) and Nokia Bell Labs, under the projects Wireless for Verticals (WIVE) and 5G Radio Systems Research, and by the Academy of Finland (under the projects 276378, 288670, and 304147).

978-9-0827-9703-9/19/$31.00 ©2019 IEEE

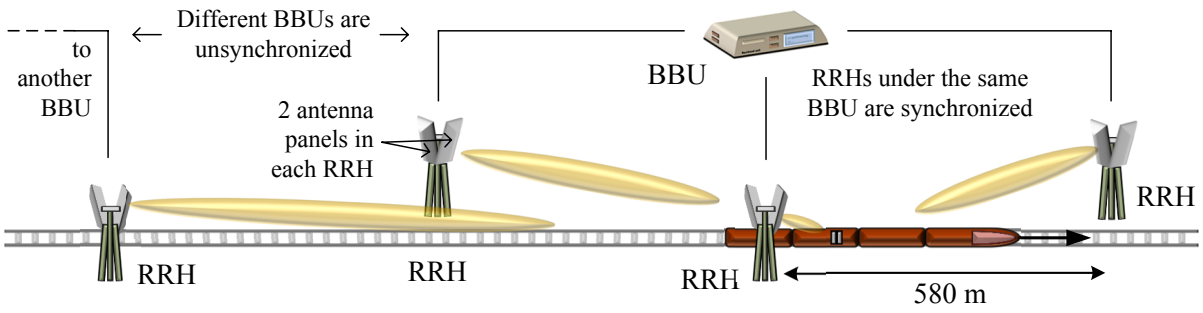

Fig. 1. Illustration of the considered high-speed railway scenario composing of multiple RRHs and BBUs, as proposed by the 3GPP in [4].

m intervals alternating between both sides of the track, as illustrated in Fig. 1. Each RRH includes two antenna panels, which are installed with 45 degree angle with respect to the track normal covering both track directions. Also the train includes two antenna panels facing towards the nose and tail of the train. As described in [4, Section 6.1.5], the network is based on a single-frequency principle, where RRHs operate in the same frequency band at 30 GHz carrier frequency.

The proposed positioning approach is based on the uplink sounding reference signal (SRS), specified in [10, Section 6.4.1.4], transmitted by the train at regular intervals. Thereon, the m^{th} received sample at the k^{th} RRH is given as

$$z_k[m] = \mathbf{b}_{\text{RX},k}\left(\gamma_k[m]\mathbf{\Lambda}_k[m]\mathbf{b}_{\text{TX}}u[m-\zeta_k] + \mathbf{n}_k[m]\right), \quad (1)$$

where $u[m-\zeta_k]$ is the m^{th} transmitted signal sample with a fractional sample delay $\zeta_k \in \mathbb{R}_+$, which allows received signals to include arbitrary time delays without limitations due to sample rate. Moreover, the received signal with a fractional sample delay is defined as

$$u[m-\zeta_k] = \sum_{q=0}^{N_{\text{slot}}-1} u[q]\text{sinc}(m-q-\zeta_k), \quad (2)$$

where N_{slot} is the number of samples in the transmitted signal, and $\zeta_k = F_{\text{s}}\tau_k$ is the radio propagation delay given in fractional samples, where F_{s} is the sampling frequency and τ_k is the radio propagation delay for the line of sight (LoS) path of the k^{th} RRH. Furthermore, $\mathbf{n}_k[m] \in \mathbb{C}^{N_{\text{RX}}}$ is white Gaussian noise for each receiver antenna element, and $\mathbf{b}_{\text{TX}} \in \mathbb{C}^{N_{\text{TX}}}$ and $\mathbf{b}_{\text{RX},k} \in \mathbb{C}^{N_{\text{RX}}}$ are the steering vectors of the transmitter (i.e., the train) and the receiver (i.e., the RRH) beamformers, respectively. The effect of path loss and shadowing is modeled by a a scaling factor $\gamma[m]_k$ based on the urban micro (uMI) scenario with LoS described in [11]. Moreover, the spatial channel matrix $\mathbf{\Lambda}_k[m]$ models fast fading effects according to the Clustered Delay Line D (CDL-D) model with root mean square delay spread of 100 ns, and a spatial power delay profile as specified in [11, Table 7.7.1-4]. Each propagation path cluster modeled with $\mathbf{\Lambda}_k[m]$ incorporate the propagation delay with respect to the delay of the LoS path τ_k. In order to match the geometry of the CDL-D model with specific transmission angles between the train and RRHs, we use the angle scaling method, specified in [11, Section 7.7.5.1].

III. Estimation of TDoA and AoA Measurements

The estimation of both AoA and TDoA is carried out at the active BBUs based on the full band uplink (UL) SRS transmitted in a periodic manner by the device. In order to relax tight synchronization requirements between the device and the network, the TDoA-based approach is considered over the time of arrival (ToA)-based approach. However, for the sake of generality, it is assumed that the BBUs have mutually different constant clock offsets, whereas the RRHs under the same BBU are considered to be mutually synchronized. In addition, we assume that the beam alignment between the train and RRHs is obtained by using an exhaustive beam training principle, where different combinations of uplink and downlink beams are compared, and the beam pair with the highest received power is chosen. Thus, the train transmits multiple SRS symbols with each available beam, and the RRHs use different receive beams per a repeated set of SRS symbols in order find the best available receive beam.

A. Estimation of Propagation Delays with Clock Errors

The TDoA measurements are based on the cross-correlation between the received signal and the known SRS signal transmitted by the train. Hence, the cross-correlation function observed in the k^{th} RRH for the i^{th} beam can be written as

$$r_{k_i}[l] = \sum_{m=0}^{N_{\text{SRS}}-1} u^*_{\text{SRS}}[m-l]z_k[m], \quad (3)$$

where m and N_{SRS} are the sample index and the number of samples in the SRS symbol, and $u_{\text{SRS}}[m]$ is the known SRS. Now, the propagation delay estimate at the k^{th} RRH can be obtained by finding the sample index, where the absolute value of the correlation function is maximized as

$$\hat{l}_k = \arg\max_l |r_k[l]| \text{ and } \hat{\tau}_k = \frac{\hat{l}_k}{F_{\text{s}}}, \quad (4)$$

where F_{s} is the sampling frequency, and $\hat{l}_k$ and $\hat{\tau}_k$ are the estimated propagation delay in samples and in seconds, respectively. Here, it should be emphasized that due to the clock error between the train and the network, $\hat{\tau}_k$ does not reflect the true propagation delay, but it is merely a pseudo-measurement used in the following steps of the TDoA method.

B. Estimation of AoA measurements

The AoA estimation utilized in this paper is based on the correlation between the received signal and known UL SRS at each RRH. Building on the similar approach as in [9], we define a weight vector as $\mathbf{w}_k = [w_{k_1}, w_{k_2}, \ldots, w_{k_N}]^{\mathrm{T}}$, where

$$w_{k_i} = \frac{\hat{\xi}_{k_i}}{\sum_{j \in \Omega_{\text{largest}}} \hat{\xi}_{k_j}}, \quad \text{with} \quad \hat{\xi}_{k_i} = \max_{l} \tilde{r}_{k_i}[l] \tag{5}$$

where $\tilde{r}_{k_i}[l]$ is the correlation function that correponds to the i^{th} beam at the k^{th} RRH, and Ω_{largest} is the set of k_N beam-indices that correspond to the largest correlation function values. Thereafter, the AoA estimate can obtained using the weighted average of the most strongest beams as

$$\hat{\theta}_k[n] = \mathbf{w}_k^{\mathrm{T}}[\theta_{0,k}, \theta_{1,k}, \ldots, \theta_{N-1,k}]^{\mathrm{T}} \tag{6}$$

where $\theta_{i,k}$ is the beam orientation for the i^{th} beam at the k^{th} RRH.

IV. Positioning of High-Speed Devices

In this paper, the position estimation and tracking of high-speed devices is carried out using an EKF, which utilizes first-order Taylor series approximations in order to linearize the non-linear measurement model of the system. In addition to tracking of the two-dimensional position and velocity of the device, we seek to jointly track the clock offsets of the active and mutually unsynchronized BBUs. Therefore, the state-vector of the device at a given time-instant n is written as

$$\mathbf{s}[n] = [x[n], y[n], v_x[n], v_y[n], \boldsymbol{\rho}[n]]^{\mathrm{T}} \in \mathbb{R}^{(4+N_{\text{BBU}})\times 1}, \tag{7}$$

where $x[n]$ and $y[n]$ are the x-coordinate and the y-coordinate of the device, and $v_x[n]$ and $v_y[n]$ are the velocity of the device in the x-direction and in the y-direction, respectively. Moreover, $\boldsymbol{\rho}[n] = [\rho_1[n], \ldots, \rho_{N_{\text{BBU}}}[n]]^{\mathrm{T}} \in \mathbb{R}^{N_{\text{BBU}}\times 1}$ contains the clock offsets of active BBUs, where N_{BBU} denotes the number of active BBUs at the given time-instant.

Furthermore, we assume that the state-transition between consecutive time-instants is linear and the measurement model that relates the available measurements $\mathbf{y}[n]$ to the state of the system is non-linear. Thus, the models can be given in a general form as

$$\mathbf{s}[n] = \mathbf{F}\mathbf{s}[n-1] + \mathbf{q}[n] \tag{8}$$

$$\mathbf{y}[n] = \mathbf{h}(\mathbf{s}[n]) + \mathbf{r}[n], \tag{9}$$

where $\mathbf{F} \in \mathbb{R}^{(4+N_{\text{BBU}})\times(4+N_{\text{BBU}})}$ is the state-transition matrix, $\mathbf{h}(\cdot)$ is the non-linear measurement model function, and $\mathbf{q}[n] \sim \mathcal{N}(0, \mathbf{Q}[n])$ and $\mathbf{r}[n] \sim \mathcal{N}(0, \mathbf{R}[n])$ are the process noise and the measurement noise vectors, respectively.

At every time-instant, the EKF-based estimation process consists of the prediction phase, and in case of available measurements, the update phase. In the prediction phase, the *a priori* mean $\hat{\mathbf{s}}^-[n]$ and covariance $\hat{\mathbf{P}}^-[n] \in \mathbb{R}^{(4+N_{\text{BBU}})\times(4+N_{\text{BBU}})}$ are obtained after propagating the previous *a posteriori* mean $\hat{\mathbf{s}}^+[n-1]$ and covariance $\hat{\mathbf{P}}^+[n-1]$ according to the state-transition model as

$$\begin{aligned} \hat{\mathbf{s}}^-[n] &= \mathbf{F}\hat{\mathbf{s}}^+[n-1] \\ \hat{\mathbf{P}}^-[n] &= \mathbf{F}\hat{\mathbf{P}}^+[n-1]\mathbf{F}^{\mathrm{T}} + \mathbf{Q}. \end{aligned} \tag{10}$$

In particular, it is assumed that the device mobility is driven by a constant white noise acceleration (CWNA) model, similar to the one used in [7], whereas the clock offsets of the active BBUs are assumed to be constant over time. Hence, the state-transition matrix $\mathbf{F}$ in (8) is defined as

$$\mathbf{F} = \begin{bmatrix} \mathbf{I}_{2\times 2} & \Delta t \cdot \mathbf{I}_{2\times 2} & \mathbf{0}_{2\times N_{\text{BBU}}} \\ \mathbf{0}_{2\times 2} & \mathbf{I}_{2\times 2} & \mathbf{0}_{2\times N_{\text{BBU}}} \\ \mathbf{0}_{N_{\text{BBU}}\times 2} & \mathbf{0}_{N_{\text{BBU}}\times 2} & \mathbf{I}_{N_{\text{BBU}}\times N_{\text{BBU}}} \end{bmatrix}, \tag{11}$$

where Δt is the time interval between two consecutive states. Furthermore, we denote the variance of the clock skew process-noise as σ_α^2, although this variance is used only in the EKF in order to enable fast enough convergence of the constant BBU clock offset state-variables. Based on the aforementioned discussion, the process noise covariance matrix is given as a block diagonal matrix $\mathbf{Q} \in \mathbb{R}^{(4+N_{\text{BBU}})\times(4+N_{\text{BBU}})}$ such that

$$\mathbf{Q} = \begin{bmatrix} \frac{\sigma_{\text{a}}^2 \Delta t^3}{3}\mathbf{I}_{2\times 2} & \frac{\sigma_{\text{a}}^2 \Delta t^2}{2}\mathbf{I}_{2\times 2} & \mathbf{0}_{2\times N_{\text{BBU}}} \\ \frac{\sigma_{\text{a}}^2 \Delta t^2}{2}\mathbf{I}_{2\times 2} & \sigma_{\text{a}}^2 \Delta t \mathbf{I}_{2\times 2} & \mathbf{0}_{2\times N_{\text{BBU}}} \\ \mathbf{0}_{N_{\text{BBU}}\times 2} & \mathbf{0}_{N_{\text{BBU}}\times 2} & \mathbf{I}_{N_{\text{BBU}}\times N_{\text{BBU}}} \end{bmatrix}, \tag{12}$$

where σ_{a}^2 is the variance of the device acceleration.

Thereafter, if there are measurements available, the obtained *a priori* mean and covariance estimates are updated in the second phase of the EKF according to the well-known Kalman gain equations

$$\mathbf{K}[n] = \hat{\mathbf{P}}^-[n]\mathbf{H}[n]^{\mathrm{T}} \left(\mathbf{H}[n]\hat{\mathbf{P}}^-[n]\mathbf{H}[n]^{\mathrm{T}} + \mathbf{R}[n]\right)^{-1} \tag{13}$$

$$\hat{\mathbf{s}}^+[n] = \hat{\mathbf{s}}^-[n] + \mathbf{K}[n](\mathbf{y}[n] - \mathbf{h}(\hat{\mathbf{s}}^-[n])) \tag{14}$$

$$\hat{\mathbf{P}}^+[n] = (\mathbf{I} - \mathbf{K}[n]\mathbf{H}[n])\hat{\mathbf{P}}^-[n], \tag{15}$$

where $\mathbf{H}[n]$ is the Jacobian matrix of the considered non-linear measurement model function $\mathbf{h}(\cdot)$ evaluated at $\hat{\mathbf{s}}^-[n]$. Now, the measurement vector $\mathbf{y}[n]$ consists of both AoA and TDoA measurements and therefore, it can be written as

$$\begin{aligned} \mathbf{y}[n] &= [\hat{\boldsymbol{\theta}}[n]^{\mathrm{T}}, \Delta\hat{\boldsymbol{\tau}}[n]^{\mathrm{T}}]^{\mathrm{T}} \\ &= [\hat{\theta}_1[n], \ldots, \hat{\theta}_{N_{\text{RRH}}}[n], \Delta\hat{\tau}_1[n], \ldots, \Delta\hat{\tau}_{N_{\text{RRH}}-1}[n]]^{\mathrm{T}}, \end{aligned} \tag{16}$$

where N_{RRH} denotes the number of active RRHs at a given time-instant. Consequently, the corresponding measurement model function in (9) can be written as $\mathbf{h}(\mathbf{s}[n]) = [\mathbf{h}_\theta(\mathbf{s}[n])^{\mathrm{T}}, \mathbf{h}_{\Delta\tau}(\mathbf{s}[n])^{\mathrm{T}}]^{\mathrm{T}}$, where

$$\begin{aligned} \mathbf{h}_\theta(\mathbf{s}[n]) &= [h_{\theta,1}(\mathbf{s}[n]), \ldots, h_{\theta,N_{\text{RRH}}}(\mathbf{s}[n])]^{\mathrm{T}} \\ \mathbf{h}_{\Delta\tau}(\mathbf{s}[n]) &= [h_{\Delta\tau,1}(\mathbf{s}[n]), \ldots, h_{\Delta\tau,N_{\text{RRH}}-1}(\mathbf{s}[n])]^{\mathrm{T}}, \end{aligned} \tag{17}$$

with

$$h_{\theta,i}(\mathbf{s}[n]) = \text{acrtan}\left(\frac{y[n] - y_i}{x[n] - x_i}\right) \tag{18}$$

$$h_{\Delta\tau,j}(\mathbf{s}[n]) = \frac{\Delta\mathbf{p}_j[n] - \Delta\mathbf{p}_{k_{\text{REF}}}[n]}{c} + \rho_{j^*}[n] - \rho_{k^*_{\text{REF}}}[n],$$

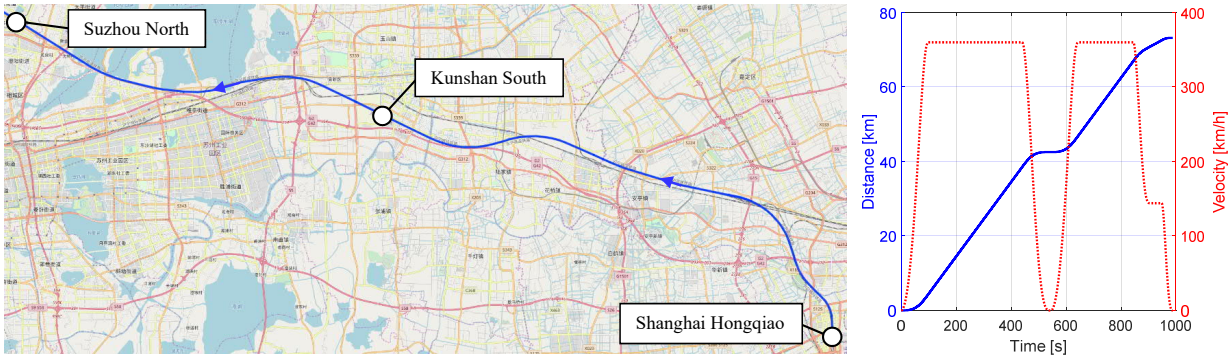

Fig. 2. The considered test track profile on the Shanghai-Beijing high-speed railway based on data obtained from [12], and the corresponding train dynamics including the travelled distance and the velocity as a function of time.

where $\Delta\mathbf{p}_j[n] = \|\mathbf{p}[n]-\mathbf{p}_j\|$ is the distance between the device and the j^{th} RRH, $\Delta\mathbf{p}_{k_{\text{REF}}}[n] = \|\mathbf{p}[n]-\mathbf{p}_{k_{\text{REF}}}\|$ is the distance between the device and the reference RRH, and c is the speed of light. Furthermore, $\rho_{i^*}[n]$ is the unknown clock offset of the $i^{*\,\text{th}}$ BBU, and $\mathbf{p}_i = [x_i, y_i]^{\text{T}}$ is the known two-dimensional location of the i^{th} RRH, respectively.

Given the measurement model function, it is straightforward to show that entries of the Jacobian matrix $\mathbf{H}[n] = [\mathbf{H}_\theta[n], \mathbf{H}_{\Delta\tau}[n]]^{\text{T}} \in \mathbb{R}^{(2N_{\text{RRH}}-1)\times(4+N_{\text{BBU}})}$ in (13) can be written as

$$\mathbf{H}_\theta[n] = \begin{bmatrix} \eta^{(x)}_{\theta,1} & \eta^{(y)}_{\theta,1} & \mathbf{0}_{1\times(2+N_{\text{BBU}})} \\ \vdots & \vdots & \vdots \\ \eta^{(x)}_{\theta,N_{\text{RRH}}} & \eta^{(y)}_{\theta,N_{\text{RRH}}} & \mathbf{0}_{1\times(2+N_{\text{BBU}})} \end{bmatrix} \tag{19}$$

$$\mathbf{H}_{\Delta\tau}[n] = \begin{bmatrix} \eta^{(x)}_{\Delta\tau,1} & \eta^{(y)}_{\Delta\tau,1} & \mathbf{e}^{*}_{(3)}{}^{\text{T}} \\ \vdots & \vdots & \vdots \\ \eta^{(x)}_{\Delta\tau,N_{\text{RRH}}-1} & \eta^{(y)}_{\Delta\tau,N_{\text{RRH}}-1} & \mathbf{e}^{*}_{(2+N_{\text{RRH}}-1)}{}^{\text{T}} \end{bmatrix},$$

where $\mathbf{e}_{(i)}$ is a vector containing zeros except the i^{th} element being equal to one, $\mathbf{e}^{*}_{(i)} = \mathbf{e}_{(i^*)} - \mathbf{e}_{(k^*_{\text{REF}})}$ denotes the partial derivatives for the BBU clock offsets, and

$$\begin{aligned} \eta^{(x)}_{\theta,i} &= -\frac{\hat{y}^-[n]-y_i}{\|\hat{\mathbf{p}}^-[n]-\mathbf{p}_i\|^2}, \qquad \eta^{(y)}_{\theta,i} = \frac{\hat{x}^-[n]-x_i}{\|\hat{\mathbf{p}}^-[n]-\mathbf{p}_i\|^2}, \\ \eta^{(x)}_{\Delta\tau,i} &= \frac{\hat{x}^-[n]-x_i}{c\|\hat{\mathbf{p}}^-[n]-\mathbf{p}_i\|} - \frac{\hat{x}^-[n]-x_{k_{\text{REF}}}}{c\|\hat{\mathbf{p}}^-[n]-\mathbf{p}_{k_{\text{REF}}}\|}, \\ \eta^{(y)}_{\Delta\tau,i} &= \frac{\hat{y}^-[n]-y_i}{c\|\hat{\mathbf{p}}^-[n]-\mathbf{p}_i\|} - \frac{\hat{y}^-[n]-y_{k_{\text{REF}}}}{c\|\hat{\mathbf{p}}^-[n]-\mathbf{p}_{k_{\text{REF}}}\|}. \end{aligned} \tag{20}$$

Finally, the measurement noise covariance matrix is determined as $\mathbf{R}[n] = \text{blkdiag}(\mathbf{R}_\theta[n], \mathbf{R}_{\Delta\tau}[n]) \in \mathbb{R}^{(2N_{\text{RRH}}-1)\times(2N_{\text{RRH}}-1)}$, where the AoA part is given as $\mathbf{R}_\theta[n] = \text{diag}(\hat{\sigma}^2_{\theta,1}, \ldots, \hat{\sigma}^2_{\theta,N_{\text{RRH}}})$ and the TDoA part as $\mathbf{R}_{\Delta\tau}[n] = \hat{\sigma}^2_{\tau,k_{\text{REF}}}\mathbf{I} + \text{diag}(\hat{\sigma}^2_{\tau,1}, \ldots, \hat{\sigma}^2_{\tau,N_{\text{RRH}}-1})$, stemming from [13].

V. Simulations and Numerical Evaluations

The performance of the proposed positioning and tracking approach for high-speed vehicles is evaluated based on the HST scenario with a curved 73 km long railway track between Shanghai and Suzhou, which is part of the Shanghai-Beijing high-speed railway. Moreover, the track coordinates are obtained from [12], and the train acceleration profiles are based on polynomial models in order to obtain more realistic train dynamics compared to constant acceleration modeling. After accelerating from the Shanghai Hongqiao station to full speed of 360 km/h, the train stops at the Kunshan South station, and after 5 s, continues towards the Suzhou North station. The considered track profile along with the travelled distance and velocity as a function of time is illustrated in Fig. 2.

The train transmits the uplink SRSs at 100 ms intervals, and the 5 closest RRHs are taken into account in trying to measure the signals. Due to noise, shadowing, and fading, it is possible that measurements are occasionally unavailable at certain RRHs. For simplicity, elevation differences are not considered, and the number of azimuth antenna elements in the train panel is defined as 4, and in the RRH panel as 16. However, in practice there could also be antenna elements in the elevation domain, which would be observed as an increased beamforming gain. Moreover, the available beam directions are defined so that the beam gain is allowed to reduce 1 dB from the maximum beam gain, when moving from one beam to another. Each BBU manages 3 adjacent RRHs, which are assumed to be synchronized with each other. However, separate BBUs have clock offsets, which are assumed to be within one frame duration as $\rho_{j^*} \in [-10, 10]$ ms. In addition, at the beginning of the simulation, the train position at the station is assumed to be known within 1 m accuracy. Consequently, the initial estimates for the BBU clock offsets and the train position are obtained randomly from the given parameter domains based on uniform distribution.

In Fig. 3, the cumulative distribution of the train position estimation error and BBU clock offset root mean squared error (RMSE) are shown for different sets of system parameters, including positioning based on both TDoA and AoA, and only TDoA. By utilizing only the beam-power-based AoA measurements for positioning is not enough to obtain sensible positioning and tracking accuracy, and therefore, it is not considered in this paper. However, AoA measurements improve the positioning performance over the TDoA-only approach, but

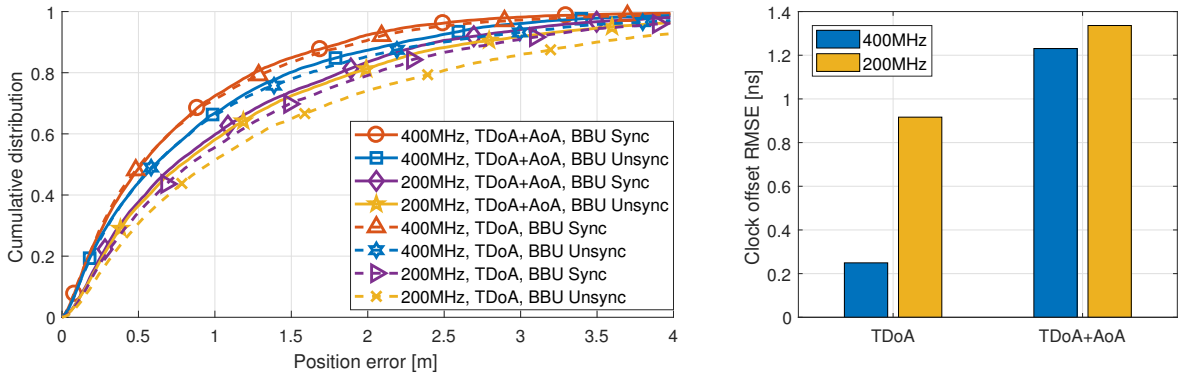

Fig. 3. Cumulative position estimation error and BBU clock offset estimation RMSE with different positioning approaches and system bandwidths.

may push some of the errors into BBU clock offset estimates. The results are shown for two separate bandwidths, including 200 MHz (i.e. 132 physical resource blocks) and 400 MHz (i.e. 264 physical resource blocks), and as a reference, positioning error results are also shown for the cases with perfect BBU synchronization. With the 400 MHz bandwidth and using both TDoA and AoA, the train position estimation error with unsynchronized BBUs is less than 2.8 m for 95% of the time, whereas with the 200 MHz bandwidth the corresponding error is roughly 3.6 m. Thus, the required below 3 m positioning accuracy with 95% availability for traffic monitoring and control systems, specified by the 3GPP, can be achieved with the 400 MHz bandwidth. However, with the 200 MHz bandwidth, or using only TDoA in case of unsynchronized BBUs, the given positioning requirements are not reached.

As shown in Fig. 3, the BBU clock offset RMSE is at at a nanosecond level for both 200 MHz and 400 MHz bandwidths, where the 400 MHz bandwidth provides slightly improved performance. Moreover, considering a sample duration, one nanosecond synchronization accuracy corresponds with approximately 0.25 samples and 0.5 samples in the 200 MHz bandwidth and 400 MHz bandwidth, respectively. Although by using both TDoA and AoA enables the best positioning accuracy, using only TDoA achieves improved clock estimation RMSE. However, overall by including AoA measurement in the EKF improves the positioning performance and the relative error between the position estimate and clock offset estimates can be adjusted by configuring the element values of the measurement covariance matrix.

VI. Conclusion

In this paper, we studied network-side radio positioning and tracking of high-speed devices in 5G NR networks without requiring specific network synchronization, which considerably enhances the practical feasibility of the proposed approach. In order to demonstrate the performance of the proposed methods, we considered a HST scenario with realistic system parameterization including coordinates of real high-speed railway track between Shanghai and Beijing.

Based on the TDoA and AoA measurements obtained from the uplink SRS transmitted by the train, we utilized EKF-based approach for joint train position estimation and network clock-offset synchronization. Based on the extensive simulation on the 73 km long high-speed railway track, we evaluated the train positioning performance for the 3GPP-specified 5G NR high-speed scenario. The results showed that with the 400 MHz utilizing both TDoA and AoA measurements, the proposed approach is able to achieve 2.8 m positioning accuracy with 95% availability, which is below the positioning accuracy requirements specified by the 3GPP for traffic monitoring and control systems. Thus, regardless of network synchronization errors, radio-based positioning for high-speed vehicles can greatly benefit various intelligent transportation systems, and provides a substantial asset for future mission-critical systems with autonomous vehicles.

References

[1] T. Levanen *et al.*, "Location-Aware 5G Communications and Doppler Compensation for High-Speed Train Networks," in *Proc. 2017 EuCNC*, June 2017, pp. 1–6.

[2] R. Di Taranto *et al.*, "Location-Aware Communications for 5G Networks: How location information can improve scalability, latency, and robustness of 5G," *IEEE Signal Process. Mag.*, vol. 31, no. 6, pp. 102–112, Nov 2014.

[3] "3GPP TR 22.872 V16.1.0 Study on positioning use cases (Release 16)," Sept. 2018.

[4] "3GPP TR 38.913 v14.3.0 Technical Specification Group Radio Access Network; Study on Scenarios and Requirements for Next Generation Access Technologies (Rel. 14)," June 2017.

[5] H. Wymeersch *et al.*, "5G mmWave Positioning for Vehicular Networks," *IEEE Wireless Commun.*, vol. 24, no. 6, pp. 80–86, Dec 2017.

[6] X. Cui *et al.*, "Vehicle Positioning Using 5G Millimeter-Wave Systems," *IEEE Access*, vol. 4, pp. 6964–6973, 2016.

[7] M. Koivisto *et al.*, "Joint Device Positioning and Clock Synchronization in 5G Ultra-Dense Networks," *IEEE Trans. Wireless Commun.*, vol. 16, no. 5, pp. 2866–2881, May 2017.

[8] B. Zhou, A. Liu, and V. Lau, "Successive Localization and Beamforming in 5G mmWave MIMO Communication Systems," *IEEE Trans. Signal Process.*, vol. 67, no. 6, pp. 1620–1635, March 2019.

[9] J. Talvitie *et al.*, "Positioning of high-speed trains using 5G new radio synchronization signals," in *2018 IEEE Wireless Communications and Networking Conference (WCNC)*, April 2018, pp. 1–6.

[10] "3GPP TS 38.211 V 15.3.0 Technical Specification Group Radio Access Network, NR Physical channels and modulation (Rel. 15)," Sept. 2018.

[11] "3GPP TR 38.901 v14.3.0 Study on channel model for frequency spectrum above 6 GHz (Release 14)," Dec. 2017.

[12] OpenRailwayMap. [Online]. Available: www.openrailwaymap.org/

[13] S. Sand, A. Dammann, and C. Mensing, *Positioning in Wireless Communications Systems*, 1st ed. Wiley Publishing, 2014.